E&P / Tommi Rämä

5 February 2024 NUCL-4846

Distribution

Reviewed by, Date
Timo Toppila, 12.2.2024

Approved by, Date
Olli Viljakainen, 13.2.2024

Electronically reviewed and approved original is in Fortum ProjectWise-program.

Replace

SAFER2023, CERESA SUBPROJECT
SIMULATIONS OF THE SELECTED CONAN EXPERIMENTS WITH ANSYS FLUENT

TABLE OF CONTENTS

1 INTRODUCTION....2
2 CONTAINMENT MODEL....2
3 CFD MODEL DESCRIPTION....3
3.1 Geometry....4
3.2 Computational grid....5
3.3 Physical and numerical models....7
3.4 Material properties....8
4 SIMULATION CASES....8
5 RESULTS....9
5.1 Case P10-T30-V15....9
5.2 Case P20-T50-V30-H08....10
5.3 Case P05-T40-V06-H62....11
6 CONCLUSIONS....12
7 REFERENCES....13

© Fortum 2022

E&P / Tommi Rämä 5 February 2024 NUCL-4846

1 INTRODUCTION

The containment system of a Pressurized Water Reactor (PWR) serves as the final barrier against the release of radioactive materials in the event of an accident or malfunction within the reactor core. Understanding and analyzing this containment system is essential to safeguarding the well-being of not only the workers at the nuclear facility but also the public at large. Containment analysis plays a pivotal role in assessing and enhancing the resilience of these structures, thereby minimizing the risk of catastrophic incidents and mitigating the consequences of severe accidents.

In the past, the containment analyses at Fortum have been carried out with COCOSYS, MELCOR and APROS system codes. Now that the detailed three-dimensional CFD (Computational Fluid Dynamics) codes and the computer power developed rapidly over the last years, the application of CFD for reactor scale containment analyses has become possible.

2 CONTAINMENT MODEL

The main goal of this project is to model hydrogen behaviour in NPP containments with CFD. In order to find out the most important phenomena that needs to be taken into account, Phenomena Identification and Ranking Table (PIRT) was made based on a hypothetical LOCA accident on Loviisa VVER-440 NPP to guide the model development. Ranking input was asked from project personnel, SAFER TAG 2.1 and other stakeholders. Readiness of the OpenFOAM models is based on the view of the project personnel, as well as the timetable for the model development. The ranking, readiness and the timetable are shown below in Table 1.

© Fortum 2022

Table 1. Phenomena identification ranking table and their readiness of the OpenFOAM models.

	Ranking by weighted average	Readiness (Ready / Needs some work / Needs to be implemented / Implemented in another project)	Timetable
Condensation at ice surfaces.	3.00		2023
Ice melting.	3.00		2024
Stratification.	3.00		-
Thermal mixing.	3.00		-
Recombinators.	3.00		2024-2025
Effect of non-condensable gases on condensation.	3.00		2023
Effect of non-condensable gases on stratification.	2.83		-
Igniters.	2.83		2025 (or not at all)
Hydrogen combustion.	2.83		2025 (or not at all)
Condensation on walls.	2.67		2023
Turbulence modelling.	2.67		-
Heat transfer between fluids and structures.	2.50		2023
Pressure losses in ice condenser.	2.33		2024
Water pools.	2.33		2024
Bulk condensation.	2.20		2024
Mist formation/evaporation.	2.17		2024
Behaviour of gas/liquid surfaces.	2.17		2024
Aerosol transport and deposition.	2.00		-
Condensation on the water pools.	2.00		2024
Water films at surfaces.	1.83		2024-2025
Thermal radiation.	1.83		-
Water droplets.	1.80		2024
Mist rainout.	1.67	No model needed.	-
Dissolution of the hydrogen.	1.50		Not at all
Mist deposition.	1.50		2024

3 CFD MODEL DESCRIPTION

The first step is to validate surface condensation model and the effect of the non-condensable gases on the condensation, mentioned in the Table 1. In this report simulations are made with Ansys Fluent CFD model with earlier developed condensation models used for example in Rämä et al. (2019). The results are compared with measurements and to some extent against OpenFOAM results from VTT (Syrjänen & Hovi 2023).

© Fortum 2022

3.1 Geometry

Following depiction is strictly quoted from Syrjänen & Hovi (2023):

“The CONAN test facility consists of primary test channel for gas phase, a cooled plate for condensation as one of its vertical sides, and secondary coolant channel on the other side of the plate. The primary test channel is 2 m in length and 0.34 m X 0.34 m in horizontal cross section. The cooled side plate is 4.5 cm thick aluminium implying 0.34 m X 0.045 m horizontal cross section. The rear side of the plate is cooled by coolant flowing in secondary coolant channel with 5 mm depth, and hence 0.34 m X 5 mm horizontal cross section, respectively.”

“The air and steam mixture enters in the primary channel from above through honeycomb panels to ensure uniform flow at the inlet. The honeycomb structure consists of three 35 mm thick panels with 3 mm honeycomb cell diameter. Condensation takes place on the cooled side plate surface, and condensate flows downward along it. The air and steam mixture exits the channel with the condensed liquid from the bottom, where the condensate is collected at the bottom of the cooled plate. The sides of the primary channel are considered adiabatic except for the cooled side plate.”

“The coolant enters the secondary coolant channel from the bottom. It flows upwards, exiting at the top of the coolant channel.” For this study 3D CFD model of the CONAN experimental facility according to Figure 1 is made.

© Fortum 2022

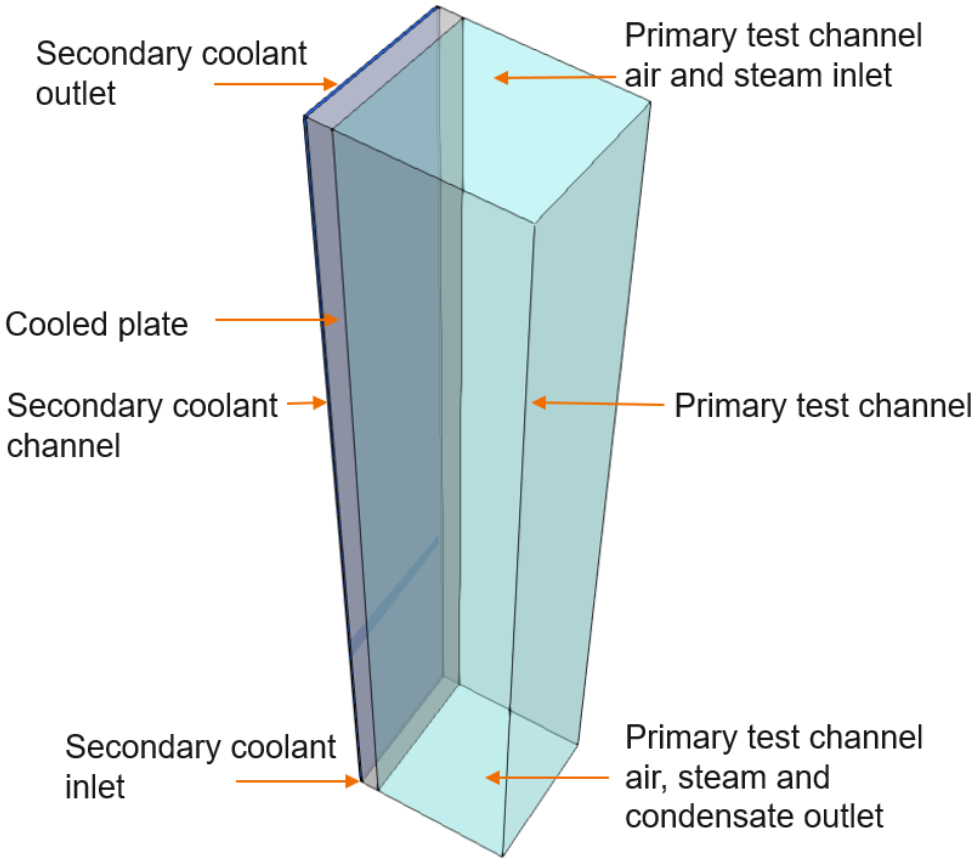

Figure 1. CONAN test device. The primary test channel for air and steam mixture shown in light blue, the cooled plate shown grey, and the coolant channel shown dark blue. (from Syrjänen & Hovi 2023)

3.2 Computational grid

Two different computational grids were used. First one was made with Fluent meshing tool. Grid consists of polygonal, prism and wedge cells. Total amount of the cells is 2.9 million. General view of the computational grid is presented in Figure 2.

© Fortum 2022

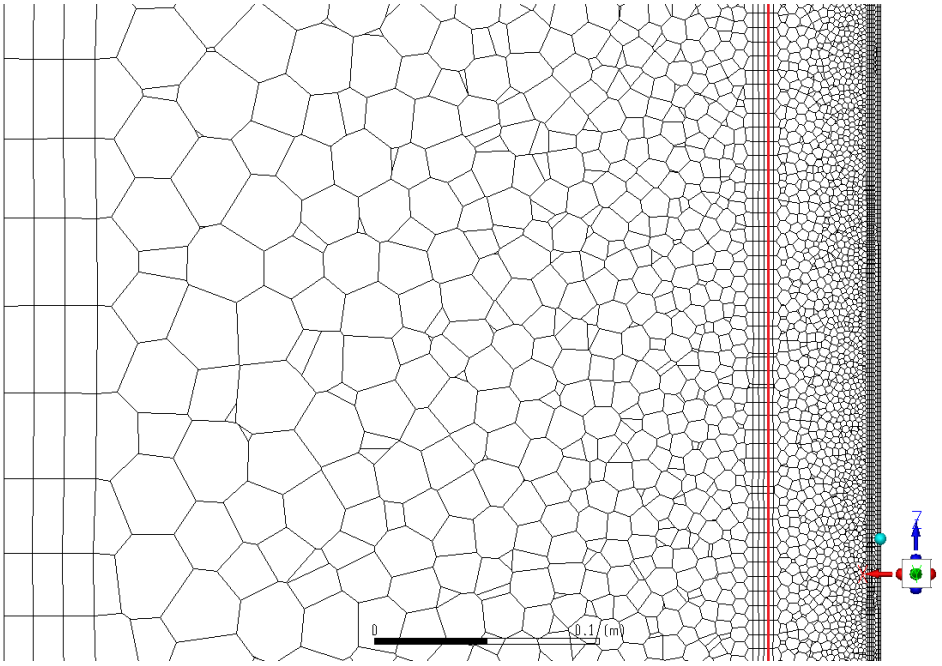

Figure 2. Hybrid computational grid. The wall between primary test channel and the aluminum plate is marked with red line. Size of the first cell from the wall is 1.1 millimeters.

The second one was purely heksahedral grid, made with Ansys Gambit. Total amount of the cells is 0.19 million. General view of the computational grid is presented in Figure 3.

© Fortum 2022

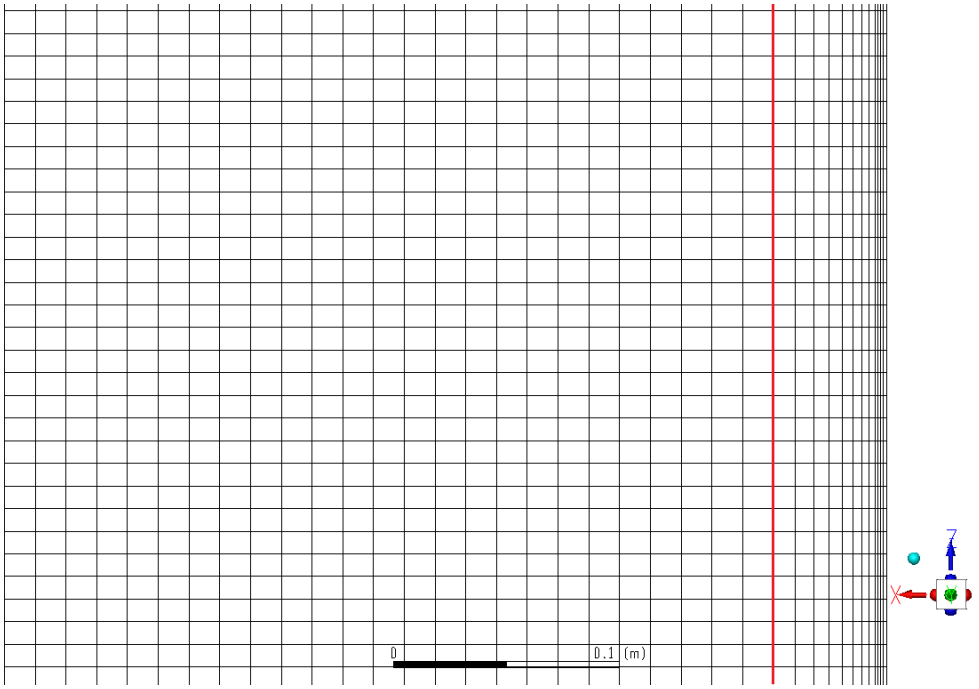

Figure 3. Heksahedral computational grid. The wall between primary test channel and the aluminum plate is marked with red line. Size of the first cell from the wall is 7.0 millimeters.

In addition, based on the results from Syrjänen & Hovi (2023) two other grids with heksahedral meshes ($0.74 \cdot 10^6$ cells and $0.08 \cdot 10^6$ cells) were made to see the mesh effect on the condensation.

3.3 Physical and numerical models

Numerical solver models were selected according to references (Siccama 2015, Visser 2015a and Visser 2015b). For pressure-velocity coupling *PISO* scheme, with *Skewness Correction* 1 and *Neighbor Correction* 1, is applied. For pressure *Body Force Weighted* scheme is applied. For all other variables *Second Order Upwind* method is used. Turbulence is modelled with *standard k-ε* model with enhanced wall treatment. Analyses are made with transient solver with constant time-step of 0.1 s.

Ansys Fluent solver version 2021R2 was used for the simulations. It solves basic fluid flow, temperature and turbulence fields and species transport. (Ansys 2021) In addition solving the following phenomena was addressed via user-defined-functions (UDFs) (Siccama 2015):

- wall deposition and evaporation
- bulk condensation and evaporation
- mist formation and rainout

Single-phase modelling, with condensation modelled with volumetric and wall reactions, was used. Steam, mist, helium and air were modelled as different species.

© Fortum 2022

3.4 Material properties

Temperature dependent material properties based on Visser (2015b) were used for vapour, mist and deposited water. Temperature dependent material properties from Icropera&DeWitt (1996) were used for air.

Table 2. Properties of water-vapor.

Temperature (K)	Specific heat (J/(kg·K))	Thermal conductivity (W/(m·K))	Viscosity (kg/(m·s))
290	1902.3	0.018031	$0.9641 \cdot 10^{-5}$
380	2053.2	0.025561	$1.2525 \cdot 10^{-5}$
500	1981.6	0.035865	$1.7269 \cdot 10^{-5}$
600	2026.9	0.046368	$2.1407 \cdot 10^{-5}$

Table 3. Properties of air.

Temperature (K)	Specific heat (J/(kg·K))	Thermal conductivity (W/(m·K))	Viscosity (kg/(m·s))
290	1007	0.0255	$1.81 \cdot 10^{-5}$
450	1022	0.0363	$2.51 \cdot 10^{-5}$
600	1052	0.0457	$3.07 \cdot 10^{-5}$

Table 4. Properties of helium.

Temperature (K)	Specific heat (J/(kg·K))	Thermal conductivity (W/(m·K))	Viscosity (kg/(m·s))
290	5193	0.15236	$1.947 \cdot 10^{-5}$
450	5193	0.20659	$2.6359 \cdot 10^{-5}$
600	5193	0.25240	$3.221 \cdot 10^{-5}$

4 SIMULATION CASES

The simulated experiments are selected according to which public information was available. The boundary conditions for the cases are from Silde (2013), Lee & Cho (2019) and Bucci et al. (2013).

Three calculation cases were simulated. First, P10-T30-V15 was with only air and steam, and it was also simulated by Syrjänen & Hovi (2023). Second case was with

© Fortum 2022

air, steam and small amount of helium, P-20-T50-V30-H08, while in the third case, P05-T40-V06-H62 the proportional amount of helium was increased but the total inlet flow velocity was decreased. The inlet boundary conditions for the simulated cases are presented in Table 5.

Table 5. Boundary conditions of the calculation cases. *v* means velocity, *T* temperature and *W* mass fraction, respectively.

Case	v_{in} (m/s)	T_{in} (°C)	W_{air}	W_{helium}
P10-T30-V15	1.5	82	0.600	-
P20-T50-V30-H08	3.11	92	0.402	0.005
P05-T40-V06-H62	0.6	76.9	0.416	0.093

For the coolant flow approximate temperature of 30°C from Ambrosini et al. (2008) was used.

5 RESULTS

The condensation rate and boundary heat flux in the middle of the coolant wall are presented with comparison against experimental results, when possible. The experimental results are digitized from Silde (2013), Bucci et al. (2013) and Lee & Cho (2019).

5.1 Case P10-T30-V15

In the experiment P10-T30-V15 the inlet flow consists of steam and air, there are no other non-condensable gases. Same experiment is also simulated by Syrjänen & Hovi (2023). The amount of the condensate is presented in Table 6 for the experiment, openFOAM and Ansys Fluent simulations. The results of the experiment and openFOAM are from Syrjänen & Hovi (2023).

Table 6. Condensation rate.

Case	**Cell count**	**Average y^+ value**	**Condensation rate (g/s)**	**Difference**
Experiment	-	-	2.3	-
OpenFOAM 20.0mm (Syrjänen & Hovi 2023)		-	2.3	-0.82 %
Ansys Fluent-hybrid-1.1mm	$2.92 \cdot 10^6$	8	2.2	-3.80 %
Ansys Fluent-heksa-7.0mm	$0.19 \cdot 10^6$	40	2.0	-13.0%
Ansys Fluent-heksa-0.4mm	$0.74 \cdot 10^6$	3	1.0	-56.5%
Ansys Fluent-heksa-11.4mm	$0.08 \cdot 10^6$	61	1.7	-26.1%

© Fortum 2022

As another comparison variable the surface heat flux along the middle of the cooling wall (cooled plate in Figure 1) was compared. In Figure 4 the comparison of the simulation (case *Ansys Fluent-hybrid-1.1mm*) and experiments is presented.

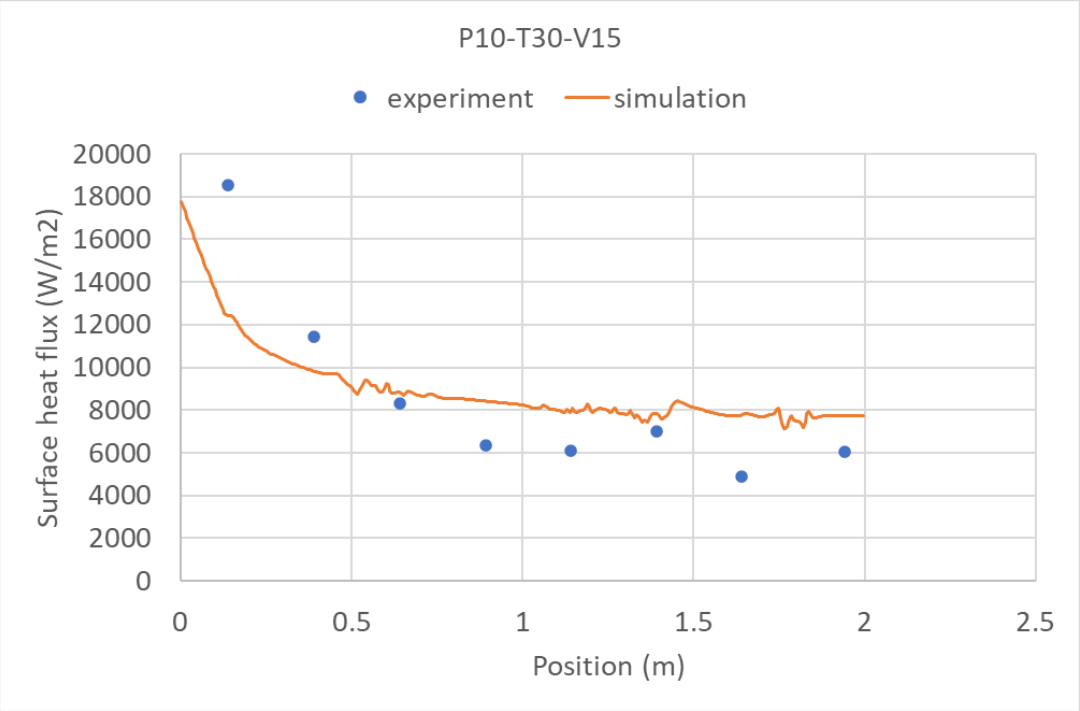

Figure 4. Surface heat flux in case P10-T30-V15.

5.2 Case P20-T50-V30-H08

In the experiment P20-T50-V30-H08 also helium is injected. Selected flow velocity leads to forced convective situation. No buoyant effects took place in the experiment. The amount of the condensate is presented in Table 7 for the experiment and Ansys Fluent simulations. The results of the experiment is approximated from Bucci at al. (2013).

Table 7. Condensation rate.

Case	Cell count	Average y^+ value	Condensation rate (g/s)	Difference
Experiment	-	-	5.2	-
Ansys Fluent-hybrid-1.1mm	$2.92 \cdot 10^6$	13	4.6	-11.5%
Ansys Fluent-heksa-7.0mm	$0.19 \cdot 10^6$	73	5.9	+13.5%
Ansys Fluent-heksa-0.4mm	$0.74 \cdot 10^6$	5	1.8	-65.4%
Ansys Fluent-heksa-11.4mm	$0.08 \cdot 10^6$	111	4.6	-11.5%

© Fortum 2022

As another comparison quantity the surface heat flux along the middle of the cooling wall (cooled plate in Figure 1) was compared. In Figure 4 the comparison of the simulation (case *Ansys Fluent-hybrid-1.1mm*) and experiments is presented.

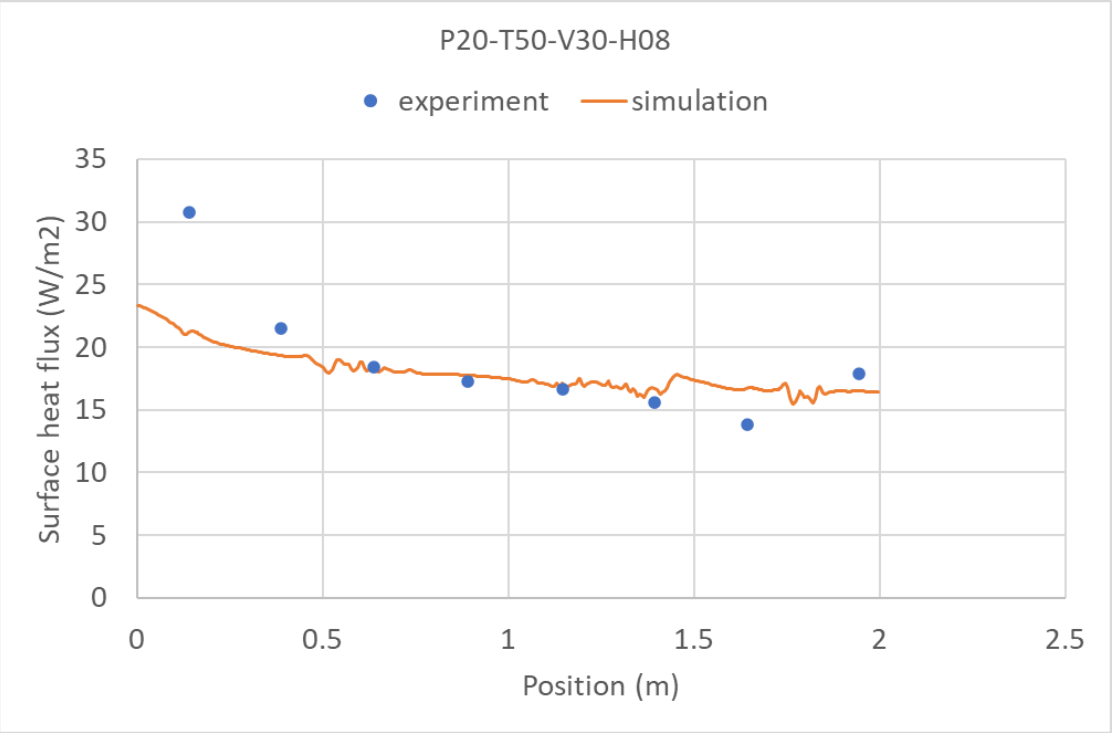

Figure 5. Surface heat flux in case P20-T50-V30-H08.

5.3 Case P05-T40-V06-H62

In the experiment P20-T40-V06-H62 steam, air and helium is injected. The flow velocity is lower than in the experiment P20-T50-V30-H08, so that the conditions change from forced convection to natural convection in the experiments. The amount of the condensate is presented in Table 8 for the Ansys Fluent simulations. The results of the experiment were not available for the author of this document.

Table 8. Condensation rate.

Case	Cell count	Average y^+ value	Condensation rate (g/s)	Difference
Experiment	-	-	not available	-
Ansys Fluent-hybrid-1.1mm	$2.92 \cdot 10^6$	3	1.1	-
Ansys Fluent-heksa-7.0mm	$0.19 \cdot 10^6$	13	1.1	-
Ansys Fluent-heksa-0.4mm	$0.74 \cdot 10^6$	1	0.7	-
Ansys Fluent-heksa-11.4mm	$0.08 \cdot 10^6$	19	0.9	-

© Fortum 2022

As another comparison quantity the surface heat flux along the middle of the cooling wall (cooled plate in Figure 1) was compared. In Figure 4 the comparison of the simulation (case *Ansys Fluent-hybrid-1.1mm*) and experiments is presented.

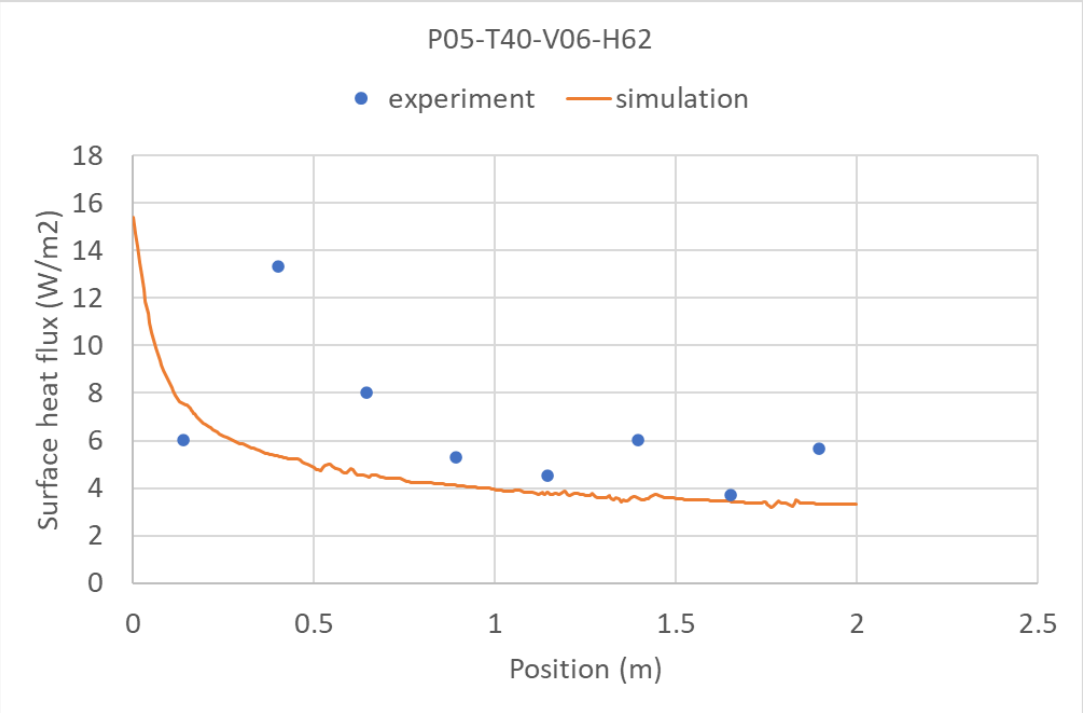

Figure 6. Surface heat flux in case P05-T40-V06-H62.

6 CONCLUSIONS

The condensation rates simulated here shows that the results are dependent on the mesh density. With selected meshes the results have fairly good agreement with the experiments, but with dense meshes the results differ clearly from the experiments. When comparing the surface heat fluxes, there are clear differences especially near the inlet. One reason might be that the modelled domain starts directly at the inlet of the cooled plate, making the flow field at the inlet possibly slightly different. As for the natural convection case, the simulations were not able to catch the surface heat flux peak at 0.4 m from inlet. Similar discrepancies were reported also by Lee & Cho (2019). Similar behaviour regarding the computational grid sensitivity on the results as in Syrjänen & Hovi (2023) was noticed.

© Fortum 2022

7 REFERENCES

Bucci, M., Ambrosini, W., Forgione, N. 2013. Experimental and Computational Analysis of Steam Condensation in the Presence of Air and Helium. Nuclear Technology, 181:1. Taylor & Francis Group. doi: 10.13182/NT13-A15761.

Ambrosini, W., Oriolo, F., Forgione, N., Paci, S. 2008. Comparison and Analysis of the Condensation Benchmark Results. The 3rd European Review Meeting on Severe Accident Research (ERMSAR-2008) Nesseber, Vigo Hotel, Bulgaria, 23-25 September 2008. [www.researchgate.net, visited 4.9.2023]

ANSYS Fluent, 2021. ANSYS Fluent User's Guide. Release 2021R2. ANSYS, Inc. www.ANSYS.com.

Lee, C. W., Cho, H.K. 2019. Computational analysis of wall condensation in the presence of non-condensable gas mixture containing a light gas with CUPID. Transactions of the Korean Nuclear Society Spring Meeting Jeju, Korea, May 23-24, 2019.

Rämä, T., Toppila, T., Visser, D.C., Siccama, N.B. 2019. Validation of ice condenser model for CFD analysis of VVER-440 type containment. Nuclear Engineering and Design volume 352. Elsevier B.V. https://doi.org/10.1016/j.nucengdes.2019.110163.

Siccama, N.B. 2014. Fortum Ice Condenser Model in Fluent. NUCLEARRD-4-2659. Fortum Power and Heat Oy.

Silde, A. 2013. Calculation of CONAN steam condensation experiments with APROS containment model. VTT research report VTT-R-07918-13. VTT Technical Research Centre of Finland.

Syrjänen, J., Hovi, V. 2023. OpenFOAM model for the analysis of hydrogen transport in NPP containment. VTT research report VTT-R-00884-23.

Visser, D. 2015a. Validation of CFD Model against Victoria Experiment-27. CFD Model Validation. NUCLEARRD-4-2511. Fortum Power and Heat Oy.

Visser, D. 2015b. Validation of CFD Model against Victoria Experiment-44. CFD Model Validation. NUCLEARRD-4-2536. Fortum Power and Heat Oy.

© Fortum 2022